NUMERICAL STUDY OF OIL WELL PLUG PROCESS

Rafael José Cavalieri Feital
Pontifical Catholic University of Rio de Janeiro - Rua Marquês de São Vicente, 225 - Gávea, Rio de Janeiro - RJ, 22451-900
rafael@feital.us

Mônica Feijó Naccache
Pontifical Catholic University of Rio de Janeiro - Rua Marquês de São Vicente, 225 - Gávea, Rio de Janeiro - RJ, 22451-900
naccache@puc-rio.br

Abstract. *The plug process of an oil well is analyzed numerically. The problem consists on two fluids with different densities placed one above other: the cement plug and the drilling fluid. The higher density fluid is the cement plug, modeled as non-Newtonian, and placed above the drilling fluid, which is considered Newtonian. This unstable situation is studied using the ANSYS Fluent software. The conservation equations are solved using the Finite Volume Method, and the multiphase flow is modeled with the Volume of Fluid method. The non-Newtonian viscoplastic behavior of the cement plug is modeled with the Generalized Newtonian Fluid constitutive equation, with the Herschel-Bulkley viscosity function. The success of the operation is determined by the combination of the governing rheological and geometric parameters. The effect of the governing parameters, such as the density ratio and the viscosity ratio, are investigated for a fixed geometry and a fixed ratio between the cement plug length and diameter. Furthermore, the influence of this ratio in the process is also analyzed while others governing parameters are fixed. It is shown that the flow is highly unstable, and that the governing parameters considerably affect the operation.*

Keywords: *viscoplastic, non-Newtonian, rheology, stability, oil well plug*

1. INTRODUCTION

One of the most common operations in the oil industry is the process of plug oil wells, which is used for abandonment and recompletion, for instance. This kind of process is very unstable because the cement density is usually higher than the drilling fluid density, which means that the cement tends to move downwards until it develops a sufficient gel strength (Abdu, Naccache and Mendes, 2012). The operation will not be successful if the displacement occurs in excess, causing a contamination between the fluids. The stability of the situation is possible when the non-Newtonian fluid has a viscoplastic behavior or when the yield stress is higher than the plug weight. If the fluids were Newtonian, the upper fluid would always fall to the bottom of the well not facing any resistance.

The flow displacement is defined by the governing conservation equations during the process. When the fluids don't present a Newtonian behavior (cement slurries and drilling muds, for example), the problem is no longer simple, since these fluids present a property that Newtonian fluids don't have, known as yield stress limit, below which the fluid behaves as a solid, with no deformation.

There are many works that deal with this kind of problem or with a similar situation. For example, Kerswell (2011) studied the fluid dynamics of two fluids in a vertical and cylindrical well in order to determine which kind of flow would maximize the volumetric flow. Another work (Frigaard and Scherzer, 1998) was based on the study of parameters involved in the fluid dynamics of two fluids in an inclined well. Besides, other works focused on the improving of the plugging process studying the well inclination (Calvert, Heathman and Griffith, 1995) or emphasizing the yield stress limit ratio between the two fluids (Crawshaw and Frigaard, 1999). The problems that cause the plug failure, such as the insufficient removal of drilling fluid and the small amount of plug pumped, were also mentioned and studied in literature (Harestad et al., 1997).

This work intends to analyze the plug process in vertical wells and study the effect of rheological parameters on flow displacement and stability. The following sections present the software required to solve the governing equations, the numerical method used and the discussion about the results obtained for a certain set of parameters.

2. PROBLEM

2.1 Description

The flow studied is shown in Fig.1. The plug fluid (fluid 2) is located between the two columns of the well fluid (fluid 1). When fluid 2 is heavier than fluid 1, fluid 2 would move downward, while fluid 1 would move upward, resulting in a final stagnant situation where fluid 1 would be above fluid 2. This equilibrium situation can be represented by the following force balance equation:

$$\frac{\Delta P}{\rho_2 g L} = 1 \tag{1}$$

According to this equation, ΔP is the pressure difference between the top and lower plug surfaces, while ρ_2 is the density of the plug fluid, g is the gravity acceleration and L is the length of the plug fluid. However, when fluid 1 is lighter than the second fluid, the displacement of fluid 2 will depend on its behavior. If this plug fluid is viscoplastic, it will only flow if the yield stress can not support the plug weight, which is represented by the following equation:

$$1 - \frac{4\tau}{\rho_2 g D} - \frac{\Delta P}{\rho_2 g L} \geq 0 \tag{2}$$

In this equation, τ is the wall shear stress and D is the diameter of the tube. Converting this parameters into dimensionless parameters, we have $\tau^* = \dfrac{\tau}{\rho_2 g D}$ and $P^* = \dfrac{P}{\rho_2 g D}$. Thereby, we can re-write the last equation into a new dimensionless one:

$$1 - 4\tau^* - \Delta P^* . \frac{D}{L} \geq 0 \tag{3}$$

There are three situations that may occur, depending on the yield stress:

A. In the first situation, the yield stress is superior to the plug weight, which means that plug will not flow ($4\tau_y^* > 1$ and $\Delta P^* = 0$), considering τ_y as the yield stress limit.

B. The flow of the plug will occur when $\tau = \tau_y$ ($4\tau_y^* + \Delta P^* . \dfrac{D}{L} = 1$), which means the plug weight will not be supported by the yield stress. This is the situation studied in this work.

C. Otherwise, the yield stress is null (wall slip), which means $\Delta P^* = \dfrac{L}{D}$ at the onset.

The cement plug process is analyzed using a tridimensional geometry (Fig. 1), since the two-dimensional geometry would not represent the real situation. L_u is the length of the drilling fluid above the plug fluid, L is the length of the plug fluid, L_d is the length of the drilling fluid under the plug fluid and the length of the well studied is represented by $L_w = L_u + L + L_d$. It is important to note that, in the process studied, $L_u = 0$. Hence, $L_w = L + L_d$. Besides, $L = L_d = \dfrac{L_w}{2}$.

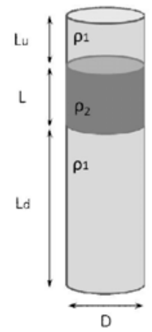

Figure 1.Tridimensional geometry

The plug fluid (dark grey), which is denser, is located between two regions containing drilling fluid (light grey). The geometry and mesh were defined using the ICEM CFD (Ansys Inc.). Having defined the geometry, the process involving the two fluids (the plug fluid and the drilling fluid) is simulated in the Fluent software (Ansys Inc.) for each case. In some cases, the drilling fluid is Newtonian while in other cases, it is non-Newtonian (following Herschel-Bulkley Model or Power-Law Model).

The conservation equations of mass and momentum are solved using the FVM (Finite Volume Method) and the PISO algorithm. The VOF (Volume of Fluid) method is used to model the multiphase flow. In this method, the volume fraction of each phase, α_i, is obtained for each phase, as described in section 2.2. As the process involves only two phases, $\alpha_1 + \alpha_2 = 1$ inside each volume control.

Considering V_C as the characteristic velocity and $\dot{\gamma}_c$ as the characteristic shear rate, we define:

$$V_C = \sqrt{gD} \qquad\qquad \dot{\gamma}_C = \frac{V_C}{D} = \frac{\sqrt{gD}}{D}$$

Since the well diameter is 1m and considering g = 9,81m/s^2, V_C = 3,13m/s and $\dot{\gamma}_C$ = 3,13s^{-1}.

The fluids have a viscoplastic behavior, then the viscosity function can be modeled by the Herschel-Bulkley model (ANSYS Inc.):

$\eta = \frac{\tau_y}{\dot{\gamma}} + K\left[\frac{\dot{\gamma}}{\dot{\gamma}_{cr}}\right]^{n-1}$ if $\dot{\gamma} > \dot{\gamma}_{cr}$, n is the Power-Law index, τ_y is the wall shear stress limit, $\dot{\gamma}$ is the shear rate and $\dot{\gamma}_{cr} = 10^{-6}\,\dot{\gamma}_c$. (4A)

$\eta = \eta_0 = \frac{\tau_y}{\dot{\gamma}}\left[\frac{2 - \frac{\dot{\gamma}}{\dot{\gamma}_{cr}}}{\dot{\gamma}_{cr}}\right] + K\left[(2-n) + (n-1)\frac{\dot{\gamma}}{\dot{\gamma}_{cr}}\right]$ if $\dot{\gamma} < \dot{\gamma}_{cr}$, η_0 is a very high viscosity. (4B)

2.2 Volume of Fluid model

The VOF model can be used as a surface-tracking technique applied to a fixed Eulerian mesh. Usually, this kind of model is used for at least two immiscible fluids when the interface between these fluids is important to be studied. A unique set of momentum equations is shared by these fluids, and the volume fraction of each one in each single cell is tracked through the domain. The sum of the volume fractions must be equal to unity. According to this model, the fluids do not mix with each other.

Any variable φ of the mixture (two fluids) can be determined by the following equation:

$\varphi = \varphi_1\alpha_1 + \varphi_2\alpha_2$, α is the volumetric fraction (5)

Considering u as the velocity, P as pressure, η as viscosity function, ρ as density, t the time and x the coordinate (unity of length), the continuity and momentum conservation equations are presented below, respectively (i, j and k are the directions):

$$\frac{\partial\rho}{\partial t} + \rho\left(\frac{\partial u_i}{\partial x_k} + \frac{\partial u_i}{\partial x_i}\right) = 0 \tag{6}$$

$$\frac{\partial \alpha_i}{\partial t} + u_i \frac{\partial \alpha_i}{\partial x_j} = 0 \tag{7}$$

$$\frac{\partial (\rho u_i)}{\partial t} + \frac{\partial (\rho u_i u_j)}{\partial x_i} = -\frac{\partial P}{\partial x_k} + \frac{\partial}{\partial x_i}\left[\eta \left(\frac{\partial u_i}{\partial x_k} + \frac{\partial u_i}{\partial x_i}\right)\right] + \rho g_k \tag{8}$$

The dimensionless governing equations are obtained for the following dimensionless variables (t_0 represents the time from which fluid movement starts):

$$t^* = (t - t_0)\dot{\gamma}_C \qquad u_i^* = \frac{u_i}{V_C} \qquad \Delta\rho^* = \frac{\Delta\rho D V_C}{\eta_C} \qquad \eta^* = \frac{\eta}{\eta_C}$$

$$x^* = \frac{x}{D} \qquad \mathrm{Re} = \frac{\rho_2 D V_C}{\eta_C}$$

Therefore, the dimensionless equations are given by:

$$\frac{\partial \rho^*}{\partial t^*} + \rho^* \left(\frac{\partial u_i^*}{\partial x_k^*} + \frac{\partial u_i^*}{\partial x_i^*}\right) = 0 \tag{9}$$

$$\frac{\partial \alpha_i}{\partial t^*} + u_i^* \frac{\partial \alpha_i}{\partial x_j^*} = 0 \tag{10}$$

$$\frac{\partial u_i^*}{\partial t^*} + \frac{\partial (u_i^* u_j^*)}{\partial x_i^*} = -\frac{\partial P^*}{\partial x_k^*}\frac{\rho_2}{\rho} + \frac{1}{\mathrm{Re}}\frac{\rho_2}{\rho}\frac{\partial}{\partial x_i^*}\left[\eta^* \left(\frac{\partial u_i^*}{\partial x_k^*} + \frac{\partial u_i^*}{\partial x_i^*}\right)\right] + 1 \tag{11}$$

2.3. Finite Volume Method technique

The governing equations are solved using the Finite Volume technique and Fluent software (ANSYS Inc.). The PISO algorithm (Patankar, 1980) was used to couple the velocity and pressure equations. The chosen mesh has 506760 elements, and it was chosen after a mesh test, comparing the results obtained with this mesh and a more refined one. As the comparison between this mesh and the more refined one presented very similar results, this mesh was the chosen one to be studied in the future cases (parametric analysis). The convergence limit was fixed in 10^{-5} for the continuity and the velocity in the three Cartesian axes. It is also important to mention that the time step size used was variable. This value is adjusted automatically to maintain the Courant Number equal to 0.25, as recommended by the literature for this kind of flow. The Courant Number is defined as a dimensionless number, which is directly proportional to the time step size and inversely proportional to the grid cell dimension.

3. RESULTS

The main goal is to obtain the minimum plug length necessary to ensure that no contamination will occur between the two fluids before the cement (plug fluid) cure (t_{cure} ~ 2 hours). Furthermore, another goal is to show the influence of the non-dimensional parameters in the process, such as the aspect ratio (L^*), density ratio ($\rho_R = \frac{\rho_2}{\rho_1}$), viscosity ratio ($\eta_R = \frac{\eta_2}{\eta_1}$) and yield stress ratio ($\tau_{y_R} = \frac{\tau_{y_2}}{\tau_{y_1}}$).

Figures 2, 4, 6 and 8 present the average interface velocity as a function of the fluid displacement time. The average interface velocity is defined as the average velocity of the interface between the plug fluid and the drilling fluid. Figs. 3, 5, 7 and 9 show how the density of the mixture at the top of the well varies with time. The influence of the non-dimensional parameters on the displacement is analyzed. The "top time" is defined as the time that is taken to the drilling fluid to pierce the wellhead. The terminal velocity $\left(u_t^*\right)$ is defined as the velocity of the quasi-steady regime (it is an arithmetic mean of the average interface velocity values that remain almost constant), while the deposition time $\left(t^*_{deposition}\right)$ is defined as the time in which the plug deposition is complete (average interface velocity is null). The numerical values of the top time, the deposition time and the terminal velocity are shown in Tab. 1, Tab. 2, Tab. 3 and Tab. 4.

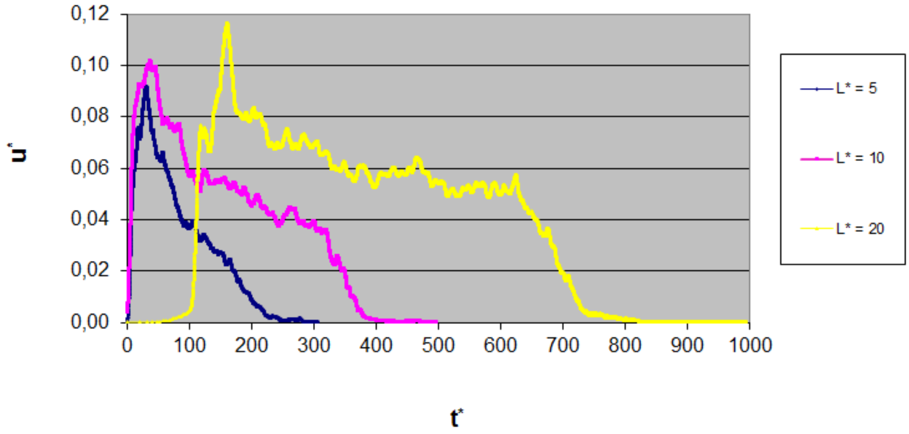

Figure 2. Average Interface Velocity vs. Time (ρ_R = 1,20, η_R = 1,00)

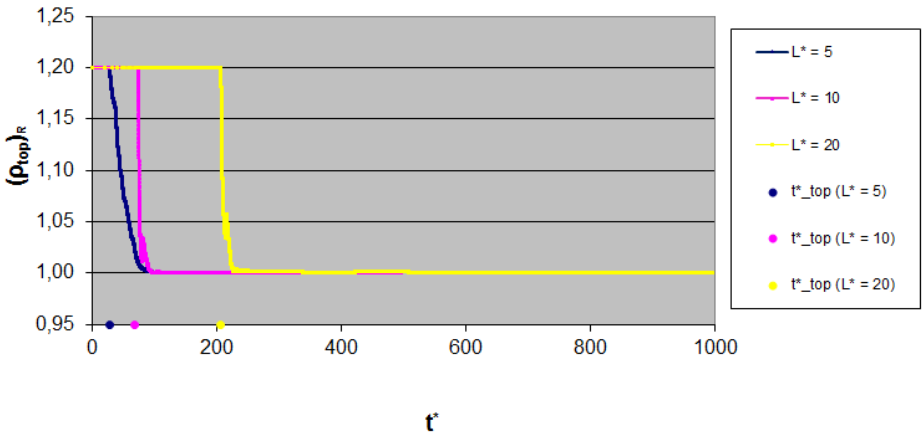

Figure 3. Density at the top vs. Time (ρ_R = 1,20, η_R = 1,00)

Table 1. Numerical results for the aspect ratio

ρ_R	η_R	L^*	t^*_{top}	$t^*_{deposition}$	u_t^*
1,20	1,00	5	28,02	299,68	-
		10	74,37	496,07	0,049
		20	206,59	973,55	0,056

Figure 2 shows that for L* = 20 and L* = 10, the interface velocity stabilizes presenting a quasi-steady regime, but this behavior does not hold for L* = 5. Also, it is observed that the terminal velocity is approximately the same for the two cases, indicating that the velocity results for L* = 10 can be used to obtain the results for a real case, where L* ~

500. Besides, the terminal velocity and the deposition time are higher as the aspect ratio increases. Figure 3 shows that the top time (it is represented in the graphic) increases as the aspect ratio also increases. The numerical results are shown in Tab. 1.

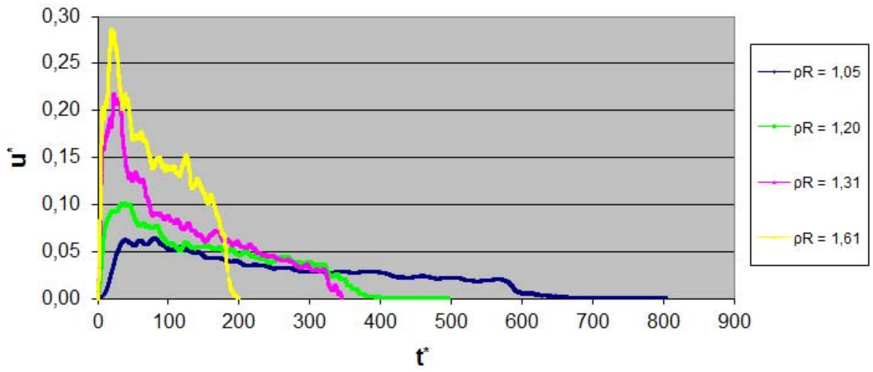

Figure 4. Average Interface Velocity vs. Time ($L^* = 10$, $\eta_R = 1{,}00$)

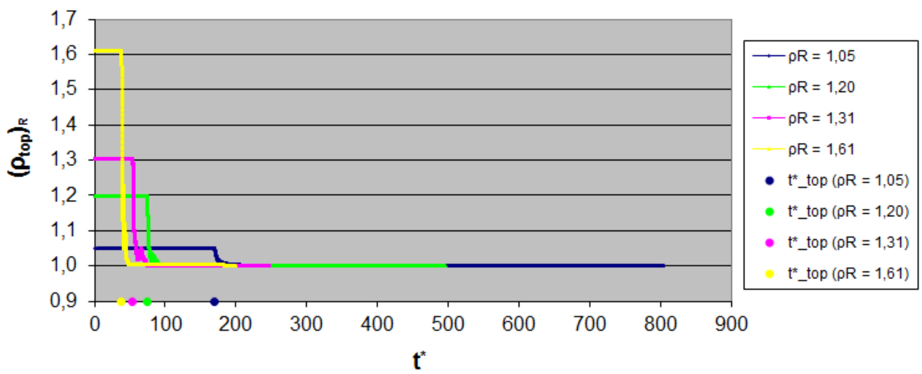

Figure 5. Density at the top vs. Time ($L^* = 10$, $\eta_R = 1{,}00$)

Table 2. Values of top time, deposition time and terminal velocity for the density ratio

L^*	η_R	ρ_R	t_{top}^*	$t^*_{deposition}$	u_t^*
10	1,00	1,05	169,33	803,67	0,028
		1,20	74,37	495,84	0,049
		1,31	54,14	345,66	0,063
		1,61	38,39	200,24	0,141

According to Figs. 4 and 5, it is concluded that the average interface velocity and terminal velocity are higher as the density ratio increases, while the top time and the deposition time increase as the density ratio decreases. The numerical results are presented in Tab. 2.

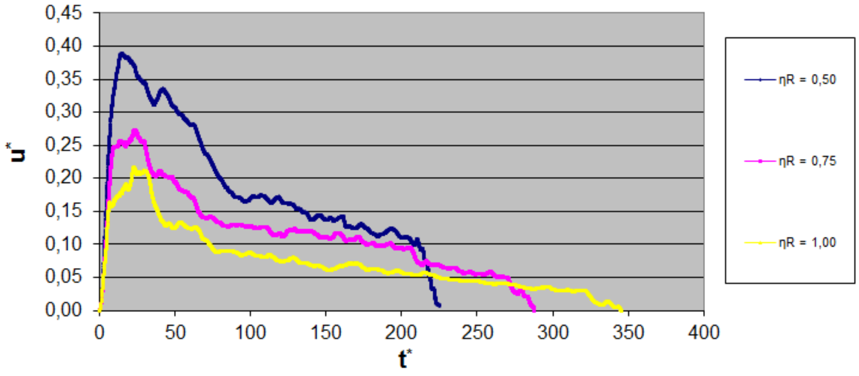

Figure 6. Average Interface Velocity vs. Time ($L^* = 10$, $\rho_R = 1{,}31$)

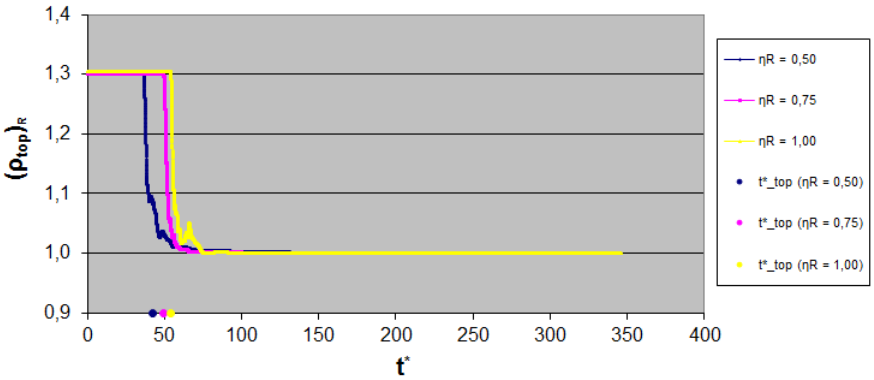

Figure 7. Density at the top vs. Time ($L^* = 10$, $\rho_R = 1{,}31$)

Table 3. Values of top time, deposition time and terminal velocity for the viscosity ratio

L^*	ρ_R	η_R	t_{top}^*	$t^*_{deposition}$	u_t^*
10	1,31	0,50	36,55	225,07	0,138
		0,75	49,57	288,05	0,131
		1,00	54,14	345,66	0,063

Figs. 6 and 7 show that the average interface velocity and the terminal velocity decrease as the viscosity ratio increases, but the top time and the deposition time increase as the viscosity ratio also increases. The numerical results are presented in Tab. 3.

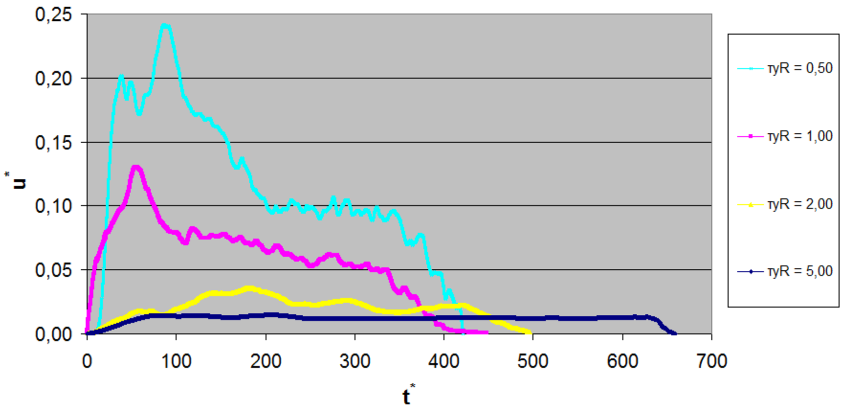

Figure 8. Average Interface Velocity vs. Time (L^* = 10, ρ_R = 1,20, η_R = 1,00)

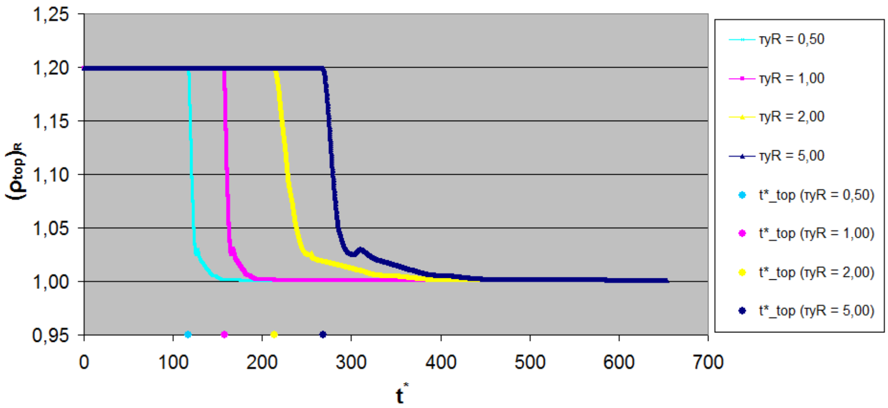

Figure 9. Density at the top vs. Time (L^* = 10, ρ_R = 1,20, η_R = 1,00)

Table 4. Numerical results for the yield stress limit ratio

L^*	ρ_R	η_R	τ_{y_R}	t_{top}^*	$t^*_{deposition}$	u_t^*
10	1,20	1,00	0,50	117,09	421,33	0,095
			1,00	157,36	448,09	0,062
			2,00	213,98	496,56	0,032
			5,00	268,15	659,16	0,019

Figs. 8 and 9 show that the average interface and terminal velocities are higher for lower yield stress limit ratio, while the top time and the deposition time decrease as the yield stress limit ratio increases. Tab. 4 presents the numerical values of the terminal velocity, top time and deposition time.

4. CONCLUSION

According to the results, it can be noted that the minimum aspect ratio necessary to guarantee that any contamination will occur before the cement cure is L^* = 10, and that the top time and the deposition time increase as the aspect ratio also increases. Besides, it can be concluded that the density ratio is inversely proportional to the top time and the deposition time, and directly proportional to the average interface velocity and the terminal velocity, while the viscosity ratio is directly proportional to the top time and the deposition time, and inversely proportional to the average interface velocity and the terminal velocity. The top time is directly proportional to the yield stress limit ratio, while the average interface velocity and the terminal velocity are inversely proportional to this ratio.

5. ACKNOWLEDGEMENTS

We would like to thank the Pontifical Catholic University of Rio de Janeiro (PUC-Rio) for the economical support, which was provided through National Council for Scientific and Technological Development (CNPq) between August of 2013 and August of 2015.

6. REFERENCES

Abdu, A., Naccache, M. F. and Mendes, P. R. S., 2012. "Effect of Rheology on Oil Well Plug Process". IMECE 2012-8614, Houston, Texas, USA, p. 1-6, 9 p.

Kerswell, R. R. "Exchange flow of two immiscible fluids and the principle of maximum flux". Journal of Fluid Mechanics, 2011, vol. 682, p. 132-159.

Frigaard, I. A.; Scherzer O. "Uniaxial exchange flows of two Bingham fluids in a cylindrical duct". IMA Journal of Applied Mathematics, 1998, vol. 61, p. 237-266.

Calvert, D. G.; Heathman, J. F.; Griffith, J. E. "Plug Cementing: Horizontal to Vertical Conditions". Society of Petroleum Engineers, 1995, SPE 30514.

Crawshaw, J. P.; Frigaard, I. "Cement Plugs: Stability and Failure by Buoyancy-Driven Mechanism". Society of Petroleum Engineers, 1999, SPE 56959.

Harestad, K. et al. "Optimization of Balanced-Plug Cementing". SPE Drilling & Completion, 1997, SPE 35084.

Fluent Users Guide, ANSYS Inc., 2012. Available in: <http://www.afs.enea.it/project/neptunius/docs/fluent/html/ug/node297.htm> Access in: 30 August 2015.

Patankar, S. V., 1980. "Numerical Heat Transfer and Fluid Flow". Hemisphere Publishing Corporation, Washington, DC.

7. RESPONSIBILITY NOTICE

The authors are the only responsible for the printed material included in this paper.